Imaging Mesoscopic Nuclear Spin Noise with a Diamond Magnetometer

Imaging mesoscopic nuclear spin noise with a diamond magnetometer

Carlos A. Meriles,[1,a)] Liang Jiang,[2,b)] Garry Goldstein,[2] Jonathan S. Hodges,[2,3,c)] Jeronimo Maze,[2] Mikhail D. Lukin,[2] and Paola Cappellaro[3]
[1]*Department of Physics, City College of New York, CUNY, New York, New York 10031, USA*
[2]*Department of Physics, Harvard University, Cambridge, Massachusetts 02138, USA*
[3]*Department of Nuclear Science and Engineering, Massachusetts Institute of Technology, Cambridge, Massachusetts 02139, USA*

(Received 27 April 2010; accepted 3 August 2010; published online 27 September 2010)

Magnetic resonance imaging can characterize and discriminate among tissues using their diverse physical and biochemical properties. Unfortunately, submicrometer screening of biological specimens is presently not possible, mainly due to lack of detection sensitivity. Here we analyze the use of a nitrogen-vacancy center in diamond as a magnetic sensor for nanoscale nuclear spin imaging and spectroscopy. We examine the ability of such a sensor to probe the fluctuations of the "classical" dipolar field due to a large number of neighboring nuclear spins in a densely protonated sample. We identify detection protocols that appropriately take into account the quantum character of the sensor and find a signal-to-noise ratio compatible with realistic experimental parameters. Through various example calculations we illustrate different kinds of image contrast. In particular, we show how to exploit the comparatively long nuclear spin correlation times to reconstruct a local, high-resolution sample spectrum. © *2010 American Institute of Physics*. [doi:10.1063/1.3483676]

I. INTRODUCTION

Physical tools have historically facilitated advances in biology; notable examples are x-rays crystallography, DNA sequencing, microarrays techniques, and, above all, microscopy in its various forms. Extending nuclear magnetic resonance (NMR) to the micro- and nanoscale promises to become another leading resource in the microscopist's toolbox. Unlike any other technique, NMR is unique in allowing the generation of images with different information content. Multidimensional high-resolution spectroscopy is today routinely used in the liquid and solid states to unveil complex molecular structures, and this capability could prove groundbreaking if samples having submicroscopic dimensions could be efficiently probed. Unfortunately, these features cannot be fully exploited at present because NMR lacks the sensitivity essential to high-resolution screening. The origin of this limitation is twofold: first, in "conventional" NMR the signal-to-noise ratio (SNR) is proportional to the nuclear magnetic polarization of the sample, which represents only a small fraction of the attainable maximum ($\sim 10^{-4}$ for protons in a 14 T magnet at 300 K). Second, Faraday induction is a poor detection method since, even with maximum polarization, the minimum number of spins needed to induce a measurable signal is comparatively large.

Although experiments performed at lower temperatures and/or higher fields can partly mitigate these problems, other more efficient detection techniques have recently been proposed. One strategy is to use the spin associated to a single nitrogen-vacancy (NV) center in diamond as a local magnetic field probe.[1,2] The operating principles of this approach closely mimic those of an atomic vapor magnetometer,[3] where the applied magnetic field is inferred from the shift in the Larmor precession frequency. Owing to the exceptionally long coherence times of NV centers, exceeding 1 ms at room temperature in ultrapure bulk samples,[4] detection of 3 nT over a measurement time of only 100 s has been experimentally demonstrated.[5] Further, a NV center within a diamond nanocrystal attached to an AFM tip was recently used to image a magnetic nanostructure with 20 nm resolution.[6]

Here we focus on applications of a NV center mounted on a scanning probe for monitoring adjacent nuclear spins in an external, infinitely extended organic sample. Rather than detecting single nuclear spins—an extremely challenging goal—we focus on the case where the NV center interacts with large ensembles of nuclear spins localized over effective volumes of 10^3–50^3 nm^3. This regime lends itself to a simplified description that simultaneously takes into consideration the quantum nature of the sensor—the NV center—while relying on a classical description of the long-range dipolar fields induced by the nuclear spin ensemble. Similar to prior magnetic resonance force microscopy experiments,[7] our strategy exploits the small dimensions of the effective sample to probe the "nuclear spin noise," i.e., the statistical fluctuations of the nuclear magnetization, rather than the magnetization itself. An important consequence is that, unlike traditional magnetic resonance imaging (MRI), spatial resolution is not due to strong magnetic field gradients but is rather determined by the distance between the NV center and the sample. Assuming a very small external magnetic field we determine the conditions required for 2D nuclear spin imaging at (or near) room temperature and show them to be

[a)]Author to whom correspondence should be addressed. Electronic mail: cmeriles@sci.ccny.cuny.edu.
[b)]Present address: Institute for Quantum Information, Caltech, Pasadena, CA 91125, USA.
[c)]Present address: Department of Electrical Engineering, Columbia University, New York, NY 10027, USA.

compatible with realistic experimental parameters. Further, we show that, in addition to determining the local nuclear spin density, this strategy allows one to explore different kinds of contrast mechanisms (nearly a requisite when imaging, for example, densely protonated organic/biological systems). In particular, we show how to reconstruct the local nuclear spin correlation function and, from it, a spatially resolved nuclear spin spectrum.

The paper is organized as follows. First, we briefly review the operating principles of NV-center-based magnetometry, more explicitly identify the effective size of the sample being probed, and lay out our detection protocol. Subsequently, we describe different modalities of nuclear spin noise detection and determine in each case the limit signal-to-noise ratio. Finally, we discuss image contrast and localized nuclear spin spectroscopy and conclude with some model calculations.

II. SPIN-NOISE MAGNETOMETRY WITH A SINGLE NV CENTER

The negatively charged nitrogen-vacancy center in diamond is an impurity comprising a total of six electrons, two of which are unpaired and form a triplet ground state with a zero-field splitting $D_{gs}=2.87$ GHz. In our calculations we assume the presence of a small magnetic field $B_A\hat{\mathbf{z}}$ (~ 10 mT) collinear with the crystal field (which, in turn, is oriented either along the [111] axis or its crystallographic equivalents). Though nonmandatory, the auxiliary field lifts the degeneracy between the $|m_s=\pm 1\rangle$ states, thus allowing one to selectively address only one of the two possible transitions, e.g., between $|m_s=0\rangle$ and $|m_s=1\rangle$.

When a green laser (532 nm) illuminates the NV center, the system is excited into an optically active triplet state; subsequent intersystem crossing produces a dark, singlet state that preferentially relaxes into $|m_s=0\rangle$. Almost complete optical pumping of the ground state takes place after a ~ 1 μs illumination, thus allowing us to model the initial density matrix of the NV center—for practical purposes, a two-level system—as

$$\rho(0) = |0\rangle\langle 0| = \tfrac{1}{2}(I + \sigma_z), \tag{1}$$

where I denotes the identity operator and σ_z is the Pauli matrix. Because intersystem crossing is allowed only if excitation takes place from $|m_s=1\rangle$, the fluorescence intensity correlates with the population of the spin state. We model the "measurement" operator as

$$M = a|0\rangle\langle 0| + b|1\rangle\langle 1| = \tfrac{1}{2}(a+b)I + \tfrac{1}{2}(a-b)\sigma_z. \tag{2}$$

In Eq. (2), a and b are two independent, stochastic variables associated with the total number of photons collected during the measurement interval (~ 300 ns) and characterized by Poisson distributions $q_a(k)=\alpha^k e^{-\alpha}/k!$ and $q_b(k)=\beta^k e^{-\beta}/k!$ with k integer. Due to the branching ratio into the dark singlet level, the averages over several measurements $\alpha \equiv \langle a\rangle$ and $\beta \equiv \langle b\rangle$ are substantially different ($\alpha \cong 1.5\beta$) and thus provide the contrast necessary to discriminate the sensor spin state.

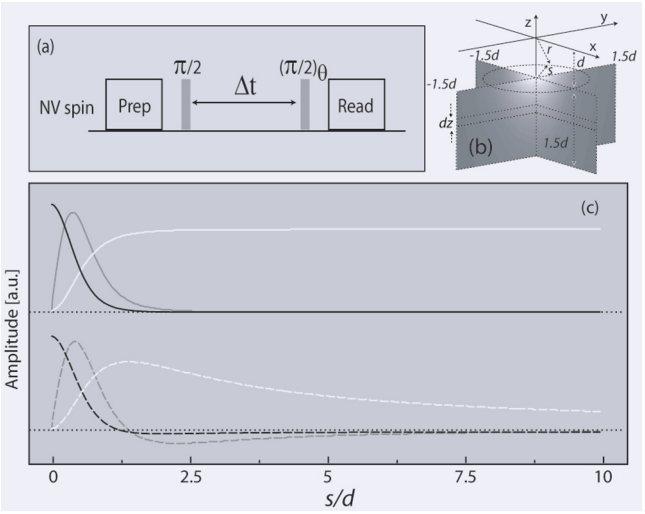

FIG. 1. (a) Basic diamond-based magnetometry pulse sequence. (b) With the NV center at the reference frame origin, the grayscale indicates the relative contribution to field fluctuations from spins in a uniformly dense film. (c) In units of the relative radial coordinate s/d, the upper set of curves shows a cross section of the graph in (b) (black curve) and the corresponding integral (white curve). The gray curve shows the effective spin noise "density" $b_N(s,z)$ (see text). For comparison, the lower set shows the same curves but for the average field at the NV center. Note that the integral (dashed white curve) decays slowly to zero as a result of negative contributions from spins far from the center.

Figure 1(a) schematically shows the basics of our detection protocol: spin initialization and a selective $\pi/2$ microwave pulse are followed by a period Δt of free evolution in the presence of an unknown, nuclear spin induced magnetic field $B_N\hat{\mathbf{z}}$. Preceding optical readout, a second $\pi/2$ pulse, shifted by a phase θ relative to the first pulse, partially converts spin coherence into population differences. In the rotating frame resonant with the chosen transition, the density matrix describing the NV center is given by

$$\rho(\Delta t) = \tfrac{1}{2}(I - \sigma_x \sin(\phi+\theta) + \sigma_z \cos(\phi+\theta)), \tag{3}$$

where $\phi = \int_0^{\Delta t} \gamma_e B_N(t)dt$ denotes the total accumulated phase due to the nuclear field and γ_e is the electronic gyromagnetic ratio. As in any other magnetometer-based strategy, the goal of a measurement is to extract the value of ϕ and, from it, valuable information on the magnetic field.

Before considering the constraints deriving from the quantum character of the sensor, we describe the magnetic field generated by the nuclear spin ensemble. In an experimental setup where the NV center scans an infinitely extended sample film, the electronic sensor spin and the nuclear spins are coupled via long-range dipolar interactions. Given that in the rotating frame resonant with the sensor spin only components of the nuclear field parallel to the z-axis need be taken into consideration, we find

$$\mathbf{B}_N = B_N\hat{\mathbf{z}} = \sum_i \{f(\mathbf{r}_i)\mathbf{m}_z^{(i)} + g(\mathbf{r}_i)(\mathbf{m}_\perp^{(i)} \cdot \hat{\mathbf{r}}_i)\hat{\mathbf{z}}\}. \tag{4}$$

Here $f(\mathbf{r}) = (\mu_0/4\pi r^3)(3\cos^2\theta - 1)$ and $g(\mathbf{r}) = (3\mu_0/4\pi r^3) \times \cos\theta$ are functions of the distance $r_i = |\mathbf{r}_i|$ of the ith nuclear spin to the NV center and θ_i is the angle between the position vector and the z-axis; μ_0 is the magnetic permeability of vacuum, and $\mathbf{m}_z^{(i)}$ ($\mathbf{m}_\perp^{(i)}$) denotes the projection of the corre-

sponding nuclear magneton $\mathbf{m}^{(i)}$ parallel (perpendicular) to the z-axis. We will consider the situation where the distance d between the sensor and the surface is of the order of ~ 10 nm or greater. We also assume that nuclear spins are dense (i.e., no nuclear spin can be singled out). In this regime, the NV center interacts with a large number of protons—exceeding 10^5 in most organic samples—and thus exerts a negligible back-action on the sample system. Each nuclear spin can be described classically via stochastic, ergodic variables featuring first and second moments $\langle m_l \rangle$ and $\langle m_l^2 \rangle$, respectively, with $l=\{x,y,z\}$.

To see that detection of the time-dependent fluctuations of the nuclear field—rather than the field itself—better suits our purpose, let us consider the example case of a uniformly magnetized film and assume, for simplicity, that the normal to the sample surface coincides with the z-axis. Using Eq. (4) we write the time-averaged field acting on the sensor as

$$\langle B_N \rangle = \frac{1}{V_p} \int_{\text{Film}} \{ f(\mathbf{r}) \langle m_z \rangle + g(\mathbf{r}) (\langle \mathbf{m}_\perp \rangle \cdot \hat{\mathbf{r}}) \} dV, \tag{5}$$

where we have transformed the sums into volume integrals via the correspondence

$$\sum_i \rightarrow \int \frac{dV}{V_p},$$

with V_p representing the volume of the "primitive cell" associated with a single nuclear spin. From symmetry considerations, we observe that the second term in Eq. (5) cancels out. This is also the case for the first term—in agreement with the classical magnetostatics result outside a thin, infinitely extended, uniformly polarized film—but here a more subtle balance between contributions from spins close and far away from the sensor is responsible.[8] The latter is shown in Fig. 1(c) where we plot $f(\mathbf{r})$ (and its integral) as a function of the (normalized) radial coordinate s on the sample plane; within each thin slice of thickness dz, long-range, weaker contributions from more numerous spins far from the sensor exactly cancel the field created by spins contained within a central disk (of diameter comparable to the sensor-slice distance).

The concept of spin noise detection capitalizes on the spontaneous fluctuations of the nuclear spin magnetization in a small volume. To more quantitatively identify the sample volume within the film, consider the special case of a uniformly distributed, infinitely extended sample and calculate the nuclear field variance $\Delta {B_N}^2$. Starting from Eq. (4) and in the limit of Eq. (5) we find

$$\Delta {B_N}^2 = \langle {B_N}^2 \rangle \cong \frac{1}{V_p} \int_{\text{Film}} \{ (f(\mathbf{r}))^2 \langle m_z^2 \rangle + (g(\mathbf{r}) \sin\theta)^2 \langle m_\perp^2 \rangle \} dV, \tag{6}$$

where we assumed $\langle m_x^2 \rangle = \langle m_y^2 \rangle = (1/2) \langle m_\perp^2 \rangle$.

Using cylindrical coordinates for convenience, we plot in Fig. 1(c) the spin noise density

$$b_N(s,z) ds dz = \frac{1}{V_p} \int_0^{2\pi} \{ [(f(s,z))^2 \langle m_z^2 \rangle + (g(s,z) s / (z^2+s^2)^{1/2})^2 \langle m_\perp^2 \rangle] s d\varphi \} ds dz.$$

While spins far from the sensor have a non-negligible contribution, fluctuations of the nuclear field at the NV center are dominated by spins approximately contained within half a sphere of radius comparable to the sensor-surface distance d. Comparing with the prior results, we conclude that fluctuations selectively highlight spins close to the sensor—as opposed to "distant" spins—not because the resulting average field is stronger but because, being less numerous, the relative field variance is larger. Finally, we emphasize that with the aid of Eqs. (5) and (6) the above reasoning can be extended without major changes to include the more general case of an irregular surface of nonuniform nuclear spin density.

A practical upper limit for the NV center-sample distance d stems from the fact that the amplitude of the field fluctuations decreases sharply with the sensor-sample distance. Assuming a sample with spin density $\rho_N \sim 1/V_p$, we find

$$\Delta B_N \sim C \mu_0 m_N \rho_N^{1/2} / d^{3/2}, \tag{7}$$

with C a constant of the order of $\sim 1/20$ obtained from integration of Eq. (6) and m_N the nuclear magneton. For example, in the case of an organic system with proton density $\rho_N \sim 5 \times 10^{28}$ m^{-3} and assuming $d \sim 200$ nm, we obtain $\Delta B_N \sim 2.5$ nT, a value approaching the sensitivity limit of a room temperature, diamond-based magnetometer.[1,5]

We note that detection of the average magnetization within the "active" volume—as opposed to magnetization fluctuations—is conceivable if the contribution to the total field from spins outside this volume has been cancelled.[8] In this case the nuclear field $\tilde{B}_N$ at the NV center site has the approximate value

$$\tilde{B}_N \sim D \mu_0 m_N \rho_N P, \tag{8}$$

independent of the sensor-surface distance. Here $P = m_N B_A / (2 k_B T)$ is the nuclear Boltzmann polarization at temperature T and D is a constant of value $\sim 1/6$. Comparing Eqs. (7) and (8) we find the criterion for spin noise dominance, $d \leq (k_B T / (m_N B_A))^{2/3} \rho_N^{-1/3}$. For example, if we take as a reference the case in which the protonated sample ($\rho_N \sim 5 \times 10^{28}$ m^{-3}) has been polarized to the equivalent of a magnetic field $B_A = 10$ T at room temperature, we have $d \leq 200$ nm.

III. SENSITIVITY LIMITS

Having identified the source and magnitude of the field fluctuations at the sensor site, we now turn our attention to the general problem of using a quantum object—the NV center—to gather information on the fluctuating ensemble of sample spins. Recalling that our observable M is the number of photons detected during a given measurement, we start by calculating the average fluorescence in the presence of the nuclear field. Combining formulas (2) and (3), we write

$$\langle \mathrm{Tr}\{M\rho\}\rangle = \tfrac{1}{2}\alpha(1+\cos\theta\langle\cos\phi\rangle) + \tfrac{1}{2}\beta(1-\cos\theta\langle\cos\phi\rangle), \quad (9)$$

where brackets indicate average over the different configurations of the nuclear system. In Eq. (9) we assume that the nuclear magnetization is negligible and that B_N (and therefore ϕ) has a symmetric distribution (i.e., $\langle\phi^{2k+1}\rangle = 0$, $k=1,2,3\cdots$). By comparison with the case in which no nuclear field is present and in the limit $\langle\phi^2\rangle < 1$, we define the signal S_A as

$$S_A \equiv \langle \mathrm{Tr}\{M\rho\}\rangle_\phi - \langle \mathrm{Tr}\{M\rho\}\rangle_{\phi=0} = (\alpha-\beta)\cos\theta\frac{(\langle\cos\phi\rangle-1)}{2}e^{-(\Delta t/T_{2e})^\gamma} \approx \frac{\langle\phi^2\rangle}{4}(\beta-\alpha)\cos\theta e^{-(\Delta t/T_{2e})^\gamma}. \quad (10)$$

In deriving Eq. (10) we introduced the coherence decay of the sensor spin characterized by the relaxation time T_{2e} and the exponent[9,10] $\gamma\sim 3$. Note that the presence of the nuclear field translates into a change of the NV center average fluorescence proportional to the nuclear spin induced phase variance. The signal amplitude also grows linearly with the difference between the average fluorescence in each of the two possible spin states and reaches a maximum value when the phase difference θ between the excitation and projection pulses is either zero or a multiple of π (see Fig. 1).

In order to determine the limiting signal-to-noise ratio, we make use of the property $M^k = a^k|0\rangle\langle 0| + b^k|1\rangle\langle 1|$ and that $\Delta a^2(\Delta b^2) = \alpha(\beta)$ for Poisson variables, to calculate the variance

$$\Delta M^2 = \langle \mathrm{Tr}\{M^2\rho\}\rangle - \langle \mathrm{Tr}\{M\rho\}\rangle^2 = \tfrac{1}{2}(\alpha+\beta) + \tfrac{1}{2}(\alpha-\beta)\cos\theta\langle\cos\phi\rangle e^{-(\Delta t/T_{2e})^\gamma} + \tfrac{1}{4}(\alpha-\beta)^2(1-\cos^2\theta\langle\cos\phi\rangle^2 e^{-(\Delta t/T_{2e})^\gamma}). \quad (11)$$

The signal-to-noise ratio, $\mathrm{SNR} = S_A/\Delta M$, is then

$$\mathrm{SNR}^{-2} = \frac{\Delta M^2}{S_A^2} = \frac{8e^{2(\Delta t/T_{2e})^\gamma}}{\langle\phi^2\rangle^2}\left\{\frac{(\alpha+\beta)+(\alpha-\beta)\cos\theta e^{-(\Delta t/T_{2e})^\gamma}}{(\alpha-\beta)^2\cos^2\theta}\right\} + \frac{4e^{2(\Delta t/T_{2e})^\gamma}}{\langle\phi^2\rangle^2}\left\{\frac{1-\cos^2\theta(1-\langle\phi^2\rangle)e^{-(\Delta t/T_{2e})^\gamma}}{\cos^2\theta}\right\}, \quad (12)$$

where, for simplicity, we have assumed $\langle\phi^2\rangle < 1$ and $\cos^2\theta \neq 0$. Note that in the limit $e^{-(\Delta t/T_{2e})^\gamma}\sim 1$ the first (otherwise dominant) term can be cancelled if we choose $\theta=\pi$ and assume that $|m_s=1\rangle$ is a "dark" state (i.e., $\beta=0$). The latter, however, is not always the case in practice because, as pointed above, we have $\alpha\cong 1.5\beta$ for direct NV spin detection. Therefore, we recast Eq. (12) in the approximate form

$$\mathrm{SNR} \approx 0.1\langle\phi^2\rangle\sqrt{\alpha}e^{-(\Delta t/T_{2e})^\gamma}, \quad (13)$$

where we made use of the fact that in current experimental settings $\alpha\cong 1.5\times 10^{-2} \ll 1$.[9,10] Hence, the optimal sensing time becomes a compromise between the increase in SNR due to larger phase change $\sqrt{\langle\phi^2\rangle}$ and the exponential decay due to decoherence. A similar sensitivity limit is obtained from the measurement of the signal fluctuation, as explained in the Appendix.

Starting from Eq. (13), we can obtain a numerical estimate of the total time T necessary for SNR=10. At a distance $d\sim 15$ nm from the surface, and for a densely protonated sample, we use Eq. (7) to find $\Delta B_N \sim 110$ nT. For a sensing interval $\Delta t\sim 40$ μs $\ll T_{2e}\sim 1$ ms we get $\langle\phi^2\rangle\cong 0.6$, thus requiring $N_A\sim 2\times 10^6$ repetitions and a total time $T_p\cong N_A\Delta t \cong 60$ s (note that in the present case $t_{\mathrm{prep}}, t_{\mathrm{read}} \ll \Delta t$, see Fig. 1). This sensitivity limit could be improved enormously if single-shot read out was available. Some strategies toward single-shot readout have recently been proposed, such as better collection efficiency via coupling of NV center to a nanophotonic wave-guide[11] or readout enhanced by a nuclear spin memory.[12,13] In this last strategy, nearby nuclear spins (such as the nitrogen associated with the NV center or a ^{13}C) are used to store the information regarding the state of the electronic NV spin, so that a given measurement can be repeated many times by mapping back the state of nuclear spin onto the electronic spin after each readout. With this technique, it is possible to further improve the SNR although at the expense of a much longer readout time (approaching several milliseconds).

IV. MEASUREMENT OF NUCLEAR SPIN TIME CORRELATIONS

In the previous section, we implicitly assume that the nuclear correlation time T_{2n} is smaller than the single measurement time (in practice, of order $\sim\Delta t$) since successive measurements must be independent if they are to improve the SNR. However, the opposite regime $T_{2n} \gg \Delta t$ allows one to extract valuable spectroscopic information on the sample system. Intuitively, this is possible because, as nuclei evolve coherently from a random initial state, the correlation function—and thus the power spectrum—of sample spins can be determined from the statistics of successive, time-delayed measurements.[14] Consistent with the assumption that the nuclear system evolves unperturbed by the NV center and that it has the effect of a classical magnetic field, we define the autocorrelation function

$$K_M(\tau) = \langle \mathrm{Tr}\{M*\rho(\Delta t+\tau)\}*\mathrm{Tr}\{M*\rho(\Delta t)\}\rangle, \quad (14)$$

with $\rho(t+\Delta t)$ denoting the density matrix that evolved under the action of the nuclear field between the times t and $t+\Delta t$ [thus acquiring the phase $\phi(t+\Delta t) = \int_t^{t+\Delta t}\gamma_e B_N(t')dt'$]. Note that since the phase acquisition takes a time Δt, we must restrict τ in Eq. (14) and thereafter to $\tau \geq \Delta t$. Combining Eqs. (14) and (2) we find

$$K_M(\tau) = \tfrac{1}{4}(\alpha+\beta)^2 + \tfrac{1}{4}(\alpha-\beta)^2(K_c(\tau)\cos^2\theta + K_s(\tau)\sin^2\theta + 2\cos\theta\langle\cos\phi\rangle), \quad (15)$$

where $K_c(\tau) \equiv \langle \cos\phi(\tau+\Delta t)\cos\phi(\Delta t)\rangle$ and $K_s(\tau) \equiv \langle \sin\phi(\tau+\Delta t)\sin\phi(\Delta t)\rangle$. Using $\phi \ll 1$, and choosing $\theta = (2k+1)\pi/2$, we recast Eq. (15) in the simpler form

$$K_M(\tau) \cong \tfrac{1}{4}(\alpha+\beta)^2 + \tfrac{1}{4}(\alpha-\beta)^2\langle\phi(\tau+\Delta t)\phi(\Delta t)\rangle. \quad (16)$$

Equations (16) and (10) can be used to reconstruct the autocorrelation function $K_\phi(\tau) \equiv \langle\phi(\tau+\Delta t)\phi(\Delta t)\rangle$ and to determine the sample power spectral density of the phase ϕ—here having the role of a stochastic variable describing a stationary random process—via the Wiener–Khintchine theorem[14]

$$F_\phi(\nu) = \int_{-\infty}^{\infty} K_\phi(\tau) e^{-i2\pi\nu\tau} d\tau. \quad (17)$$

Note that because of the finite phase acquisition time, Eq. (17) is restricted to a bandwidth defined by the inverse of the separation between two successive measurements $\sim 1/\Delta t$ (and has a central observation frequency determined by $n/\Delta t$, with n representing the number of π-pulses within the contact time Δt).

V. IMAGING AND SPECTROSCOPY OF NUCLEAR SPINS IN BIOLOGICAL SYSTEMS

In this section we consider examples that illustrate some of the potential advantages—and limitations—of using the proposed technique to reconstruct an image or a local nuclear

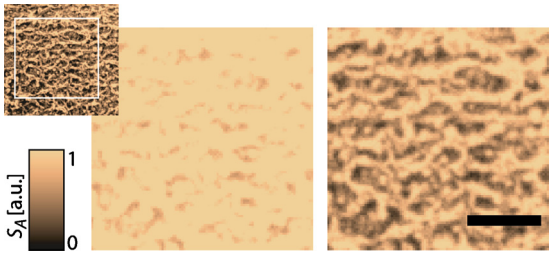

FIG. 3. (Insert) SEM image of the membrane of a red blood cell. Void spaces become apparent only after dehydration and fixation. (Main images) Simulated "raster scan" image. Unlike Fig. 2, the virtual 2D spin matrix is uniform (emulating the case of a "wet membrane"). This time the color scale of the source image was used to encode the local nuclear spin correlation time. In the example presented on the left, "mobile" regions (corresponding to dark regions in the source image) have a correlation time only 1.3 times shorter than the rest. The image on the right is based on identical conditions except that the correlation time difference was three times greater. The scale bar corresponds to 300 nm.

Δt, can be exploited to make the time-averaged phase shift ϕ negligibly small. The latter is shown in Fig. 3 where we used an SEM image from the membrane of a red blood cell to encode the correlation time of spins on a uniformly dense lattice (i.e., spins in the void spaces of the SEM image were assigned a shorter nuclear correlation time). This example provides a rudimentary model for a "water-filled" membrane whose semirigid skeleton can be distinguished from the embedded fluid.

In situations similar to that of Fig. 3, Eq. (17) could be used, for example, to monitor diffusion processes. In this context, we note that one of the most important structural characteristics of the cell membrane is that it behaves like a two-dimensional liquid, i.e., its constituent molecules rapidly move about in the membrane plane. Therefore, one could imagine extensions of the basic pulse protocol to emulate their corresponding NMR counterparts (but with resolution on the tens of nanometers). In principle, a broad range of diffusion rates is within reach (because the probing time can be greatly enhanced if, after a given evolution period, the NV center coherence is stored in an adjacent ^{13}C nucleus for future retrieval).[9] Studies of this kind may prove worthy, especially if we keep in mind that although the structure of plasma membranes is known to be inhomogeneous, the precise architecture of this important system still remains unclear.[15]

In a different implementation where the auxiliary field B_A points along an axis noncollinear with the crystal field one could rely on the above formalism to extract spectroscopic information from random nuclear spin coherences. An example is shown in Fig. 4 where we consider a set of (model) molecules with a 13 Hz heteronuclear (e.g., proton-phosphorous) J-coupling. In our simulation the auxiliary magnetic field B_A is 20 gauss, the tip distance is 30 nm, and the system correlation time is 100 ms. Assuming the sensor at a fixed position in space, Fig. 4 shows the pulse sequence and resulting autocorrelation function and power spectral density. Implicit in this model is the idea that molecules tumble and move relative to each other so as to cancel inter- and intramolecular dipolar couplings without escaping the observation volume of the sensor during Δt. Our example

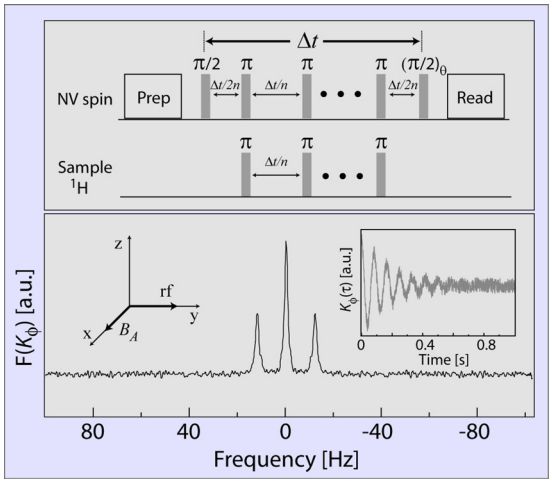

FIG. 4. In this example the NV center repeatedly monitors a set of equivalent protons subject to a 6.5 Hz heteronuclear J-coupling with a second (invisible) spin-1/2 species. Depending on the alignment of the latter, protons precess with one of two possible frequencies. (Top) Schematics of the pulse sequence; n denotes the number of π-pulses within the evolution interval Δt. (Bottom) Reconstructed correlation (insert) and corresponding spectral density. Note the factor 2 in the observed splitting (13 Hz), a direct consequence of having assumed $|\cos\theta|=1$ (quadratic response). In the simulation $n=1$, $d=30$ nm, and $\Delta t=100$ μs. The nuclear correlation time is 100 ms and the number of single measurement pairs per point in the correlation curve is 4×10^5. The external magnetic field B_A is 5 mT and pulses acting on nuclear spins are assumed to be broadband so as to invert proton spins as well as the J-coupled species. Other conditions are as listed in the text.

mimics the conditions of "restricted diffusion" found, for example, within a cell membrane where molecules "hop" between adjacent, $\sim$(100 nm)^3 compartments on a time scale of several milliseconds.[16]

VI. CONCLUSION

While high-field MRI serves as a superb tool to probe the living world, achieving submicroscopic spatial resolution presently appears to be a goal exceedingly difficult. Indirect detection via NV centers in diamond provides an alternative platform that we examined by means of analytical and numerical calculations. We considered the particular case of a single NV center interacting with a large number of nuclear spins, a condition that we described in semiclassical terms. When brought in close proximity to the sample surface, e.g., with the aid of a high-precision scanner, the NV center is selectively sensitive to field fluctuations induced by nuclear spins immediately adjacent to the sensor (even if the mean sample magnetization is negligible). The important practical consequence is that prepolarization magnet, gradient coils, and fast-switching current amplifiers—today mandatory in a nuclear spin imaging experiment—are not requisites of this technology.

Our calculations show that simple Ramsey or spin-echo sequences are able to probe the nuclear spin system although the relative phase between pulses plays a crucial role. Under current experimental conditions, photon shot noise is the main source of error. We stress, however, that the sources of this limitation are not fundamental and that technical advances could lead to significant decrease in the imaging times.

When compared to other kinds of microscopies, several distinguishing features of NV center-based magnetometry emerge. For example, given the sharp dependence on the sensor-sample distance, detection is restricted to surface spins (with the result that careful sample preparation will be necessary when inner structures of a system are to be exposed). On the other hand, the same setup could be exploited to reconstruct three-dimensional (3D) topographic maps that can then be used to enrich the information content of the images produced via the NV center fluorescence. Even if exposure times longer than those typical of other imaging schemes are necessary, diamond-based magnetometry has the potential to gauge changes in the dynamics and chemical composition of the sample, thus opening the door to various types of contrast. In particular, we have shown that, with an adequate protocol, one could probe molecular diffusion or reconstruct the low- or zero-field nuclear spin spectrum[17,18] with nanoscale spatial resolution. Finally, we note that most biochemical reactions are thermally driven, stochastic processes that involve the crossing of a barrier or diffusion over some kind of potential energy surface. Therefore, the ability to conduct experiments in an open environment, at room temperatures can prove crucial to expose the dynamics of living systems in ways not possible with traditional magnetic resonance. For example, with spatial resolution of ~5 nm—only slightly better than our target here—one could envision investigating the stepping of single molecular motors, a process that usually takes place in the tens of milliseconds range.

ACKNOWLEDGMENTS

We are thankful to Vik Bajaj for useful comments and to David Cowburn for their remarks on large portions of this manuscript. C.A.M. acknowledges support from the Research Corporation and from NSF. L.J. acknowledges support from Sherman Fairchild Fellowship. Work at Harvard is supported by the NSF, DARPA, and the Packard Foundation.. P.C. acknowledges support from NIST award #60NANB10D002.

APPENDIX: MONITORING SPIN NOISE VIA THE FLUORESCENCE VARIANCE

While through Eq. (10) we monitor sample spins via changes in the average number of photons emitted by the sensor, similar information can be obtained if we measure instead changes in the fluorescence variance. This strategy closely mimics that already demonstrated in magnetic force microscopy[7] and, within the framework presented above, appears as a "natural" alternate pathway. Starting from Eq. (11) and neglecting relaxation for simplicity, a simple calculation shows that the signal S_V in this case is given by

$$S_V \equiv \Delta M_\phi^2 - \Delta M_{\phi=0}^2 \cong \tfrac{1}{4}\cos\theta(\alpha-\beta)((\alpha-\beta)\cos\theta - 1)\langle\phi^2\rangle. \tag{A1}$$

To determine the limit uncertainty, we define the auxiliary operator $V \equiv (M - \langle \mathrm{Tr}\{M\rho\}\rangle)^2$ and calculate $\Delta V^2 = \langle \mathrm{Tr}\{(V - \langle \mathrm{Tr}\{V\rho\}\rangle)^2\rho\}\rangle$. In the limit in which the shot noise is stronger than the spin noise, we find after a lengthy but straightforward calculation $\Delta V^2 \cong \alpha$. Therefore, the signal-to-noise ratio is given in this case by

$$\mathrm{SNR} = \frac{S_V}{\Delta V} \cong 0.1\langle\phi^2\rangle\sqrt{\alpha}, \tag{A2}$$

in agreement with Eq. (13).

We note that S_A in Eq. (10)—and thus S_V, Eq. (A1)—is insensitive to fluctuations of the nuclear field if the phase difference θ between the excitation and projection pulses is an odd multiple of $\pi/2$. In a way, this condition is counterintuitive because, in a sequence where the pulses are phase-shifted, the magnetometer responds linearly—not quadratically—to external fluctuations, prompting the question as to whether higher sensitivity can be reached.

Though in a different context, Wineland and collaborators[19] discussed similar problems extensively. Their work highlights the ambiguity that stems from the quantum character of the sensor via the concept of quantum projection noise. When a single two-level system probes a (nonfluctuating) magnetic field, maximum sensitivity comes at the price of complete uncertainty in the outcome of a measurement; reciprocally, when the measurement variance is zero, so is the sensitivity to external fields. Although in the present case the signal comes in the form of fluctuations of the magnetometer phase, this principle does play here an important (if more subtle) role. We can make it explicit by rewriting Eq. (11) as

$$\Delta M^2 = \Delta M_q^2 + \Delta M_c^2, \tag{A3}$$

where $\Delta M_q^2 = \langle \mathrm{Tr}\{M^2\rho\} - (\mathrm{Tr}\{M\rho\})^2\rangle$ and $\Delta M_c^2 = \langle (\mathrm{Tr}\{M\rho\})^2\rangle - \langle \mathrm{Tr}\{M\rho\}\rangle^2$. The first contribution measures the quantum projection noise or uncertainty in a population measurement of a single two-level system; the second term corresponds to the nuclear spin noise-induced variance in a classical, macroscopiclike sensor (where the average polarization can be determined from a single measurement). If, for simplicity, we consider in Eq. (2) $a=1$ and $b=0$, we find after a simple calculation

$$\Delta M_q^2 = \tfrac{1}{4}(1 - \langle\cos^2(\phi+\theta)\rangle), \tag{A4}$$

and

$$\Delta M_c^2 = \tfrac{1}{4}(\langle\cos^2(\phi+\theta)\rangle - \langle\cos(\phi+\theta)\rangle^2). \tag{A5}$$

For the special case $\theta = (2k+1)\pi/2$ it follows $\Delta M_c^2 = (1/4)\times\langle\sin^2\phi\rangle$ and $\Delta M_q^2 = (1/4)(1-\langle\sin^2\phi\rangle)$ meaning that as we increase the amplitude of the external field fluctuations, the gain in the classical contribution to the variance is lost because of an equal but opposite change of the quantum projection noise. This is no longer the case when $\theta = k\pi$ thus leading to an observable change in the variance of the sensor fluorescence.

[1] J. M. Taylor, P. Cappellaro, L. Childress, L. Jiang, D. Budker, P. R. Hemmer, A. Yacoby, R. Walsworth, and M. D. Lukin, Nat. Phys. **4**, 810 (2008).
[2] C. L. Degen, Appl. Phys. Lett. **92**, 243111 (2008).
[3] D. Budker and M. Romalis, Nat. Phys. **3**, 227 (2007).
[4] G. Balasubramanian, P. Neumann, D. Twitchen, M. Markham, R. Kolesov, N. Mizuochi, J. Isoya, J. Achard, J. Beck, J. Tissler, V. Jacques, P. R. Hemmer, F. Jelezko, and J. Wrachtrup, Nature Mater. **8**, 383 (2009).

[5] J. R. Maze, P. L. Stanwix, J. S. Hodges, S. Hong, J. M. Taylor, P. Cappellaro, L. Jiang, M. V. Gurudev Dutt, E. Togan, A. S. Zibrov, A. Yacoby, R. L. Walsworth, and M. D. Lukin, Nature (London) **455**, 644 (2008).
[6] G. Balasubramanian, I. Y. Chan, R. Kolesov, M. Al-Hmoud, J. Tisler, C. Shin, C. Kim, A. Wojcik, P. R. Hemmer, A. Krueger, T. Hanke, A. Leitenstorfer, R. Bratschitsch, F. Jelezko, and J. Wrachtrup, Nature (London) **455**, 648 (2008).
[7] C. L. Degen, M. Poggio, H. J. Mamin, and D. Rugar, Phys. Rev. Lett. **99**, 250601 (2007).
[8] C. A. Meriles, J. Magn. Reson. **176**, 207 (2005).
[9] M. V. Gurudev Dutt, L. Childress, L. Jiang, E. Togan, J. Maze, F. Jelezko, A. S. Zibrov, P. R. Hemmer, and M. D. Lukin, Science **316**, 1312 (2007).
[10] L. Childress, M. V. Gurudev Dutt, J. M. Taylor, A. S. Zibrov, F. Jelezko, J. Wrachtrup, P. R. Hemmer, and M. D. Lukin, Science **314**, 281 (2006).
[11] T. Babinec, B. J. M. Hausmann, M. Khan, Y. Zhang, J. Maze, P. R. Hemmer, and M. Loncar, Nat. Nanotechnol. **5**, 195 (2010).
[12] L. Jiang, J. S. Hodges, J. R. Maze, P. Maurer, J. M. Taylor, D. G. Cory, P. R. Hemmer, R. L. Walsworth, A. Yacoby, A. S. Zibrov, and M. D. Lukin, Science **326**, 267 (2009).
[13] P. Neumann, J. Beck, M. Steiner, F. Rempp, H. Fedder, P. R. Hemmer, J. Wrachtrup, and F. Jelezko, Science **329**, 542 (2010).
[14] W. B. Davenport, *Probability and Random Processes* (McGraw-Hill, New York, 1970).
[15] B. F. Lillemeier, J. R. Pfeiffer, Z. Surviladze, B. S. Wilson, and M. M. Davis, Proc. Natl. Acad. Sci. U.S.A. **103**, 18992 (2006).
[16] K. Murase, T. Fujiwara, Y. Umemura, K. Suzuki, R. Iino, H. Yamashita, M. Saito, H. Murakoshi, K. Ritchie, and A. Kusumi, Biophys. J. **86**, 4075 (2004).
[17] R. McDermott, A. H. Trabesinger, M. Mück, E. L. Hahn, and A. Pines, Science **295**, 2247 (2002).
[18] D. P. Weitekamp, A. Bielecki, D. Zax, K. Zilm, and A. Pines, Phys. Rev. Lett. **50**, 1807 (1983).
[19] W. M. Itano, J. C. Bergquist, J. J. Bollinger, J. M. Gilligan, D. J. Heizen, F. L. Moore, M. G. Raizen, and D. J. Wineland, Phys. Rev. A **47**, 3554 (1993).